



THE UNIVERSITY *of* EDINBURGH

Edinburgh Research Explorer

Modeling fluvial incision and transient landscape evolution: Influence of dynamic channel adjustment

Citation for published version:

Attal, M, Tucker, GE, Whittaker, AC, Cowie, P & Roberts, GP 2008, 'Modeling fluvial incision and transient landscape evolution: Influence of dynamic channel adjustment', *Journal of Geophysical Research*, vol. 113, no. F3, F03013, pp. 1-16. <https://doi.org/10.1029/2007JF000893>

Digital Object Identifier (DOI):

[10.1029/2007JF000893](https://doi.org/10.1029/2007JF000893)

Link:

[Link to publication record in Edinburgh Research Explorer](#)

Document Version:

Publisher's PDF, also known as Version of record

Published In:

Journal of Geophysical Research

Publisher Rights Statement:

Final published version made available by AGU for archiving in an institutional repository. Copyright (2009) American Geophysical Union.

General rights

Copyright for the publications made accessible via the Edinburgh Research Explorer is retained by the author(s) and / or other copyright owners and it is a condition of accessing these publications that users recognise and abide by the legal requirements associated with these rights.

Take down policy

The University of Edinburgh has made every reasonable effort to ensure that Edinburgh Research Explorer content complies with UK legislation. If you believe that the public display of this file breaches copyright please contact openaccess@ed.ac.uk providing details, and we will remove access to the work immediately and investigate your claim.



Modeling fluvial incision and transient landscape evolution: Influence of dynamic channel adjustment

M. Attal,¹ G. E. Tucker,² A. C. Whittaker,¹ P. A. Cowie,¹ and G. P. Roberts³

Received 8 August 2007; revised 6 March 2008; accepted 1 April 2008; published 5 August 2008.

[1] Channel geometry exerts a fundamental control on fluvial processes. Recent work has shown that bedrock channel width depends on a number of parameters, including channel slope, and is not solely a function of drainage area as is commonly assumed. The present work represents the first attempt to investigate the consequences of dynamic, gradient-sensitive channel adjustment for drainage-basin evolution. We use the Channel-Hillslope Integrated Landscape Development (CHILD) model to analyze the response of a catchment to a given tectonic perturbation, using, as a template, the topography of a well-documented catchment in the footwall of an active normal fault in the Apennines (Italy) that is known to be undergoing a transient response to tectonic forcing. We show that the observed transient response can be reproduced to first order with a simple detachment-limited fluvial incision law. Transient landscape is characterized by gentler gradients and a shorter response time when dynamic channel adjustment is allowed. The differences in predicted channel geometry between the static case (width dependent solely on upstream area) and dynamic case (width dependent on both drainage area and channel slope) lead to contrasting landscape morphologies when integrated at the scale of a whole catchment, particularly in presence of strong tilting and/or pronounced slip-rate acceleration. Our results emphasize the importance of channel width in controlling fluvial processes and landscape evolution. They stress the need for using a dynamic hydraulic scaling law when modeling landscape evolution, particularly when the relative uplift field is nonuniform.

Citation: Attal, M., G. E. Tucker, A. C. Whittaker, P. A. Cowie, and G. P. Roberts (2008), Modeling fluvial incision and transient landscape evolution: Influence of dynamic channel adjustment, *J. Geophys. Res.*, 113, F03013, doi:10.1029/2007JF000893.

1. Introduction

[2] The occurrence and magnitude of fluvial processes such as erosion, sediment transport, and deposition, depend strongly on the stream power available per unit area of the river bed. Stream power is defined as the rate of potential energy expenditure of a body of water moving downstream. The stream power per unit area of the bed, or specific stream power, is equal to $\rho gQS/W$ where ρ = density of water, g = gravitational acceleration, Q = water discharge, S = channel slope and W = channel width. Channel geometry (e.g., slope, width) therefore exerts a fundamental control on fluvial dynamics and, as the river system is itself coupled to adjacent hillslopes, changes to channel geometry also influence the rate and style of landscape evolution as a whole [e.g., Burbank *et al.*, 1996]. While channel slopes can

be extracted from Digital Elevation Models (DEMs), the dimensions of active channel width are often lower than the DEM resolution. For that reason, empirical relationships are frequently used to estimate channel width, for example to estimate the downstream distribution of specific stream power in either natural rivers or for fluvial channels in landscape evolution models. Typically, it is assumed that channel width W scales with the square root of the discharge Q , i.e.:

$$W = k_w Q^{1/2}, \quad (1)$$

where k_w = constant. This relationship was originally defined for self-formed channels in alluvial rivers [Leopold and Maddock, 1953]. In bedrock rivers, similar scaling relations have been observed [Montgomery and Gran, 2001; Snyder *et al.*, 2003a; Whittaker *et al.*, 2007b] but equation (1) has been shown not to be valid when the relative uplift field is heterogeneous [Harbor, 1998; Lavé and Avouac, 2001; Duvall *et al.*, 2004; Finnegan *et al.*, 2005; Amos and Burbank, 2007], when contrasting lithologies are exposed [Wohl and Achyuthan, 2002] or when the landscape is in a transient state, i.e., readjusting to a change in external boundary conditions [Whipple *et al.*, 2000a; Whittaker *et al.*, 2007a]. In these contexts, equation

¹Institute of Earth Sciences, School of GeoSciences, University of Edinburgh, Edinburgh, UK.

²Cooperative Institute for Research in Environmental Sciences, and Department of Geological Sciences, University of Colorado, Boulder, Colorado, USA.

³Research School of Geological and Geophysical Sciences, Birkbeck College, and University College London, London, UK.

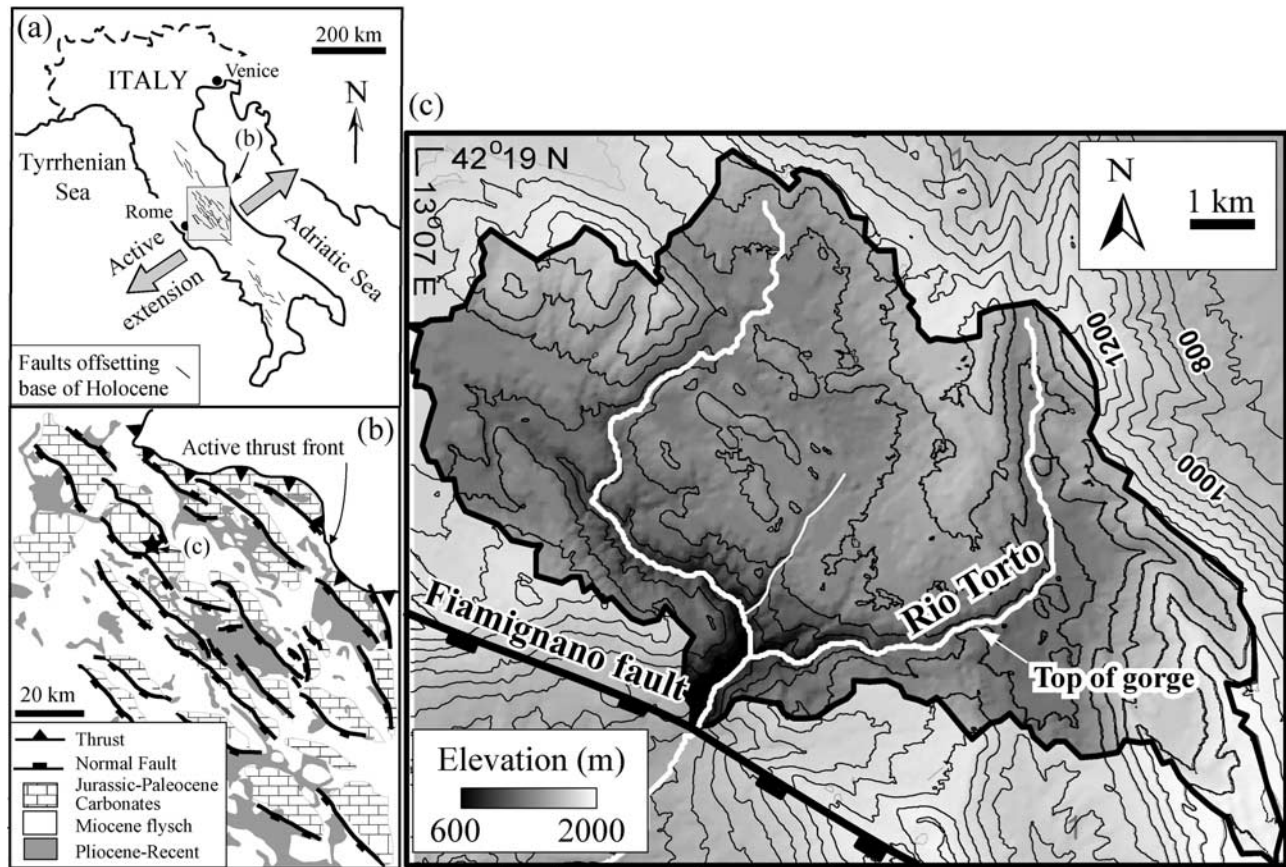


Figure 1. Location of the Rio Torto catchment analyzed in this study (modified from Whittaker *et al.* [2007b]). (a) Location map of the central Apennines, Italy. (b) Geology map of the central Apennines; star shows location of the Rio Torto catchment. (c) Map of the Rio Torto catchment. Contour spacing = 100 m.

(1) makes inaccurate predictions in terms of channel width and consequently of erosion rates. Whittaker *et al.* [2007a] showed for example that using equation (1) results in the underestimation of the real specific stream power by up to a factor of three along the Rio Torto, a river that flows across an active normal fault in the Apennines (Italy).

[3] Recent studies have focused on the geometry of bedrock channels, analytically [Finnegan *et al.*, 2005; Stark, 2006; Wobus *et al.*, 2006], experimentally [Shepherd and Schumm, 1974; Wohl and Ikeda, 1997; Carter and Anderson, 2006; Turowski *et al.*, 2006; Johnson and Whipple, 2007; Finnegan *et al.*, 2007; Douglass and Schmeckle, 2007] and in the field [Lavé and Avouac, 2001; Montgomery and Gran, 2001; Snyder *et al.*, 2003a; Duvall *et al.*, 2004; Amos and Burbank, 2007; Craddock *et al.*, 2007; Whittaker *et al.*, 2007a, 2007b]. They all stress the dynamic nature of the shape of bedrock channels and show that channel dimensions depend on a number of variables, including discharge, slope, uplift rate, vertical erosion rate, lithology, sediment supply and bed roughness. Because water tends to flow faster in steeper reaches and therefore occupy smaller channel cross sections, an increase in channel slope should lead to a reduction of channel width [Finnegan *et al.*, 2005; Wobus *et al.*, 2006; Cantelli *et al.*, 2007]. Finnegan *et al.* [2005] further hypothesized that the width-to-depth ratio and the Manning's roughness coefficient in a bedrock channel

may tend to remain constant, which implies a slope (S) dependency on channel width:

$$W = k_{wf} Q^{3/8} S^{-3/16}, \quad (2)$$

where k_{wf} = constant. Such a relationship (called “Finnegan equation” hereafter) implies that a channel narrows following a slope increase. It successfully predicts the evolution of channel width along steady state bedrock rivers experiencing uniform uplift (King Range, California) or differential uplift (Yarlung Tsangpo River, Tibet) [Finnegan *et al.*, 2005], “steady state” in this case referring to rivers along which the rate of rock uplift relative to some datum, such as mean sea level, equals the river incision rate. Equation (2) is also supported by a simple physically based model of self-formed bedrock channels [Wobus *et al.*, 2006]. In field studies of transient landscapes, it improves the predictions of channel width relative to equation (1) [Whittaker *et al.*, 2007a], even if it does not fully capture the changes in channel properties associated with transient response, such as modification of the width-to-depth ratio and bed roughness (due to variation in sediment caliber) which have been documented in the field [e.g., Whittaker *et al.*, 2007a] and experimentally [Turowski *et al.*, 2006]. Whittaker *et al.* [2007a] also proposed a modified version of

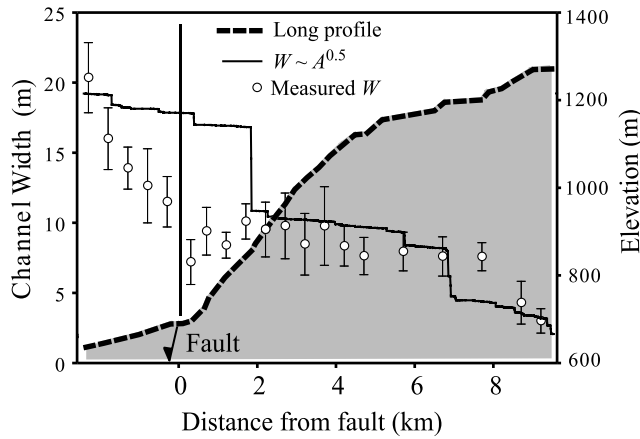


Figure 2. Long profile of the Rio Torto and field measurement of channel width along the channel (modified from Whittaker *et al.* [2007b]). Prediction of channel width using the typical hydraulic scaling relationship (equation (1)) is shown. Predictions are poor in the zone which has responded to fault acceleration (steepened reach, see Whittaker *et al.* [2007a]).

equation (2) to account for the reduction of width-to-depth ratio with increasing slope that they documented in a catchment responding to a tectonic disturbance:

$$W = k_{ww} Q^{0.38} S^{-0.44}, \quad (3)$$

where k_{ww} = constant. This empirical relationship (called “Whittaker equation” hereafter) implies that slope may be as important as drainage area for determining width in transient channels.

[4] Equations (1), (2), and (3) clearly make different predictions of the spatial and temporal evolution of channel geometry in response to changing tectonic (or climatic) boundary conditions and thus imply that there may be substantive (but currently unquantified) differences in the wider landscape as a result. Consequently, to successfully understand the influence of dynamic channel adjustment on landscape evolution, we need to know the extent to which these competing equations affect the magnitude, style and timescale of landscape response to tectonic perturbation. In this paper we address this challenge. We use the Channel-Hillslope Integrated Landscape Development (CHILD) model [Tucker *et al.*, 2001] to analyze the transient evolution of a catchment in response to a tectonic perturbation and we perform a sensitivity analysis to investigate the consequences of using a static expression for channel width (equation (1)) compared to relationships that allow for a more “realistic” dynamic adjustment of channel width to a change in slope (equations (2) and (3)). We calibrate the model to the Rio Torto catchment, Central Italian Apennines (section 2), which is known to be undergoing a transient response to accelerated fault motions, and the morphology of which has been characterized in the field [Whittaker *et al.*, 2007a]; equation (3) was also initially derived from measurements made along the Rio Torto. We exploit these data set to provide a robust initial template for the model, while varying key model boundary conditions to extract

generic information on the effect of dynamic width adjustment for different tectonic scenarios (sections 4 and 5). In particular, we characterize the differences between the topographies generated using equation (1), (2), and (3) for fault uplift which is varied temporally, spatially and in magnitude, and discuss the consequences of using inappropriate hydraulic scaling relationship on channel profile evolution, response time and landscape morphology.

2. Field Data

[5] A well-studied catchment in the footwall of an active normal fault in the central Apennines (Italy) is used as template in the present study (Figure 1). The Rio Torto catchment (drainage area = 65 km²) is located in the footwall of the Fiamignano fault. For this catchment, extensive data are available on channel and catchment morphology, on dominant erosion processes [Whittaker *et al.*, 2007a, 2007b] and on the tectonic history of the fault [Roberts and Michetti, 2004; Whittaker *et al.*, 2007b]. Mesozoic platform limestone is exposed in the footwall of the Fiamignano fault, which is a tilted fault block [Roberts and Michetti, 2004; Whittaker *et al.*, 2007b]. The fault initiated ~3 Ma with a throw rate of ~0.3 mm/a. The throw rate increased from 0.3 to 1.0 mm/a at ~0.75 Ma, due to fault interaction and linkage [Roberts and Michetti, 2004; Whittaker *et al.*, 2007b]. Whittaker *et al.* [2007a, 2007b] showed that the Rio Torto catchment is undergoing a transient response to the fault acceleration, and that this response is characterized by the development of a steepened, convex reach in the river’s long profile upstream of the fault while the upper part of the catchment is progressively uplifted and back-tilted (Figures 1 and 2). The upper part of the catchment exhibits a broad, open valley while channel narrowing has led to the formation of a gorge along the steep lower reach. The width-discharge scaling relationship (equation (1)) makes poor predictions in terms of channel width within this gorge (Figure 2) [Whittaker *et al.*, 2007a]. The development of a steepened reach in response to an increase in fault throw rate is consistent with detachment-limited stream erosion theory, which defines fluvial erosion rate as a function of specific stream power or boundary shear stress (see section 3). In addition, large and abundant bedrock exposures in the channel and fluvial Shield stress well in excess of the critical shear stress for particle entrainment suggest that the catchment behavior is close to the detachment-limited end-member [Whittaker *et al.*, 2007b].

3. Fluvial Erosion: Theory

[6] In this study, we are interested in isolating the effect of dynamic channel adjustment on landscape development. All the erosion parameters are consequently set to values that are kept constant between runs. A detachment-limited fluvial incision law is used in the model. In this case, CHILD computes the rate of vertical channel erosion E as follows:

$$E = k_b \tau^p, \quad (4)$$

where k_b = erodibility coefficient and τ = fluvial shear stress. We consider that the rate of incision is proportional to

Table 1. Values of Parameters Used in the Model

Parameter	Value
Grid spacing	~250 m
Mean storm precipitation rate P	0.75 mm/h
Mean storm duration T_r	22 h
Mean interstorm duration T_b	260 h
Catchment drainage area A	~65 km ²
Mean flood discharge at the outlet	13.6 m ³ /s
Erodibility coefficient k_b ,	$8.10^{-6} \text{ m}^{-1/2} \text{ kg}^{-3/2} \text{ s}^2$
k_b value used for runs with shear stress threshold (section 5.4)	$(\lambda = 0.15 \text{ m}),$ $10.10^{-6} \text{ m}^{-1/2} \text{ kg}^{-3/2} \text{ s}^2$ $(\lambda = 0.12 \text{ m})$
Manning's roughness coefficient n_m	0.025
Channel width coefficient	$4.6 \text{ m}^{-1/2} \text{ s}^{1/2}$
k_w (equation (1))	
Channel width coefficient	$3.2 \text{ m}^{-1/8} \text{ s}^{3/8}$
k_{wf} (equation (2))	
Channel width coefficient	$1.2 \text{ m}^{-1/8} \text{ s}^{3/8}$
k_{wv} (equation (3))	
Exponent p (equation (4))	3/2

the rate of energy dissipation per unit bed area and set p to 3/2 [Seidl and Dietrich, 1992; Howard et al., 1994; Whipple and Tucker, 1999]. More specifically, we hypothesize that the rate of mass detachment per unit bed area, $E_m = \sigma E$, scales as $E_m = \tau_0 U_* / \lambda g$, where $U_* = \sqrt{\tau / \rho}$, ρ is fluid density, σ is bedrock bulk density, g is the acceleration due to gravity, and λ is an erosion parameter that represents the work per unit weight required to detach rock. This latter parameter has dimensions of length, analogous to a hydraulic head, and is related to k_b by $1/k_b = \lambda g \sigma \sqrt{\rho}$. The scaling implied would be appropriate for determining erosion rates in a fluvial system dominated by plucking driven by bed load impact flux [Whipple et al., 2000b]. By assuming steady, uniform flow in a relatively wide channel, and applying Manning's roughness formula, the cross-section averaged boundary shear stress can be written as:

$$\tau = \rho g n_m^{3/5} (Q/W)^{3/5} S^{7/10}, \quad (5)$$

where Q = discharge = product of the runoff rate P by the drainage area A ($Q = PA$), ρ = fluid density (1000 kg.m⁻³), g = gravitational acceleration (9.81 m.s⁻²), and n_m = Manning's roughness coefficient, fixed to 0.025 in this study [for derivation, see, e.g., Howard [1994]]. Combining (4) and (5) gives:

$$E = K_1 (Q/W)^{0.9} S^{1.05}, \quad (6)$$

where $K_1 = \rho g^{1/2} n_m^{3/5} / (\lambda \sigma) = \text{constant}$. Note that, in the case in which equation (1) is used to define the channel width, and because Q is assumed to be proportional to the drainage area, equation (6) can be written:

$$E = K_2 A^{0.45} S^{1.05}, \quad (7)$$

where $K_2 = \text{constant}$. Equation (7) is a version of the commonly used stream power incision law, which implies that the general slope-area form can be derived from

stream power [e.g., Seidl and Dietrich, 1992; Whipple and Tucker, 1999]. When equation (2) is used to define channel width, a similar expression with different exponents can be derived from equation (6):

$$E = K_3 A^{0.56} S^{1.22}, \quad (8)$$

where $K_3 = \text{constant}$. When equation (3) is used to define channel width, equation (6) becomes:

$$E = K_4 A^{0.56} S^{1.45}, \quad (9)$$

where $K_4 = \text{constant}$. Note that the difference between equations (7) and (8) is not dramatic; essentially a 20% increase in the slope exponent in the latter case. On the other hand, the difference between equations (7) and (9) is notable, with a slope exponent ~40% larger when equation (3) is used to define channel width. In the following sections, we analyze the consequences of these differences for the predicted response of a catchment to a tectonic disturbance.

4. Model Setup and Steady State Topography

[7] The set of parameters used in the model is presented in Table 1. We emphasize that the wider aim of this modeling is not to reproduce in detail the evolution of the Rio Torto catchment itself but to gain general insight into how this type of footwall catchment (which is typical of an active extensional setting) might evolve in response to a tectonic disturbance, depending on the hydraulic scaling law chosen to define channel width. In CHILDR, rainfall is generated over the catchment according to a Poisson rectangular pulse rainfall model [Eagleson, 1978; Tucker and Bras, 2000]. In the model, three parameters are specified: rainfall intensity P , storm duration T_r , and interstorm duration T_b . We use values for P , T_r , and T_b typical of a Mediterranean climate, based on data from the US west coast [Hawk, 1992] (Table 1). Note that climate has been changing dramatically over the Quaternary, an era characterized by glacial-interglacial periods alternating relatively frequently. However, testing the effect of varying climate on landscape development is beyond the scope of this study: climate parameters are kept constant over the length of the runs and the same parameters are used in all the runs. For simplicity, no critical shear stress for particle entrainment (and thus erosion) is specified in this study. However, we performed several tests using a critical shear stress representative of the measured average median grain size along the Rio Torto, the results of which are presented in section 5.4. The real topography of the Rio Torto catchment was extracted from a 20-m-resolution DEM and transformed into a triangulated irregular network with a grid spacing of ~250 m (Figure 3); this grid size represents a good balance between the size of the landscape features that are analyzed and the size that allows runs to be performed in a relatively short amount of time. The boundary condition represents a tectonic scenario that is based on the reconstructed history of the Fiamignano fault which initiated ~3 Ma and the throw rate of which increased from 0.3 to 1.0 mm/a ~0.75 Ma [Roberts and Michetti, 2004; Whittaker et al., 2007b]. The tectonic setup is illustrated in Figure 3. It

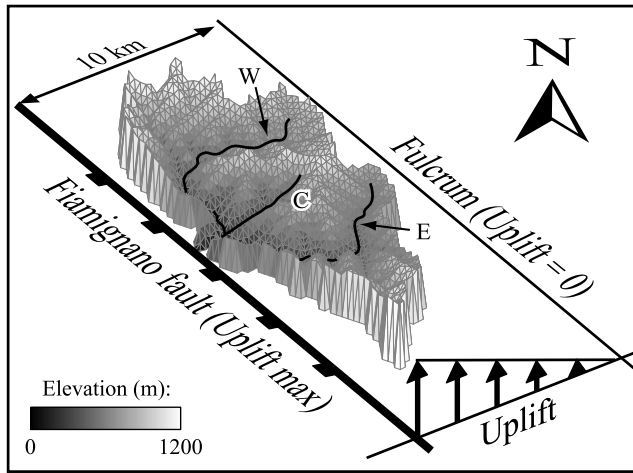


Figure 3. Model setup. The Rio Torto catchment, in the footwall of the Fiamignano fault, is used as a template for the study. The boundary of the catchment is kept fixed. The topography shown is in steady state with respect to the footwall uplift field associated with a fault throw rate of 0.3 mm/a (see text). In the model, uplift decreases linearly from fault to fulcrum (located 10 km away from fault), except for runs presented in section 5.3 in which the effect of varying pivot distance is tested. W, C, and E refer to Western, Central and Eastern channels respectively.

consists of a back-tilting footwall block associated with a relative footwall uplift rate that decreases linearly from fault to fulcrum. The use of the block-tilting model (as opposed to a flexural model) is justified in the Central Apennines by the small spacing between faults [Anders *et al.*, 1993], on average ~ 10 km [Roberts and Michetti, 2004] (Figure 1). The fulcrum position was chosen to reflect this average fault spacing. We allowed the landscape to reach a topographic steady state (i.e., erosion rate matches uplift rate at all points of the landscape) with respect to a slip-rate on the fault of 0.3 mm/a prior to imposing any fault acceleration. This is consistent with evidence from the Apennines where rivers and footwall drainage networks had become established to fault slip rates of ~ 0.3 mm/a over a time period of ~ 2 Ma [Whittaker *et al.*, 2007b]. Because the geometry of the fluvial network in the catchment was probably already established prior to fault acceleration, we applied to the modern topography the uplift field associated with a fault throw rate of 0.3 mm/a until the topography reached steady state. The response of the catchment to an increase in throw rate was then analyzed. Three cases were considered, depending on the equation chosen to estimate channel width W along the channel: the STATIC CASE refers to runs performed using the simple width-discharge scaling relationship (equation (1)); the DYNAMIC CASE refers to runs performed using the Finnegan equation (equation (2)); the DYNAMIC CASE_II refers to the runs performed using the Whittaker equation (equation (3)).

[8] To calibrate the hydraulic scaling coefficients k_w , k_{wf} , and k_{ww} (equations (1), (2), and (3) respectively), and the erodibility coefficient k_b (equation (4)) for which constraints are barely available, it makes sense to select values which provide a match to the geometry of our field template (section 2). This allows us to exclude the possibility that

our results are due to arbitrary selection of model coefficients. First, static case runs were performed, using the initial and boundary conditions outlined in the previous paragraph; k_w was set to $4.6 \text{ m}^{-1/2} \text{ s}^{1/2}$ ($\lambda = 0.15 \text{ m}$) to produce values of W which fit the measured values in the upper part of the real catchment which has not responded yet to the fault acceleration (Figures 2 and 4b). The erodibility coefficient k_b was then calibrated to produce, after fault acceleration to 1 mm/a, an average channel slope that matches the average slope over the segment of the Rio Torto that has responded to the fault acceleration (steepened reach with $S \sim 0.1$, see Figure 2 and section 5.1) [Whittaker *et al.*, 2007a]: a value of $8.10^{-6} \text{ m}^{-1/2} \text{ kg}^{-3/2} \text{ s}^2$ was used for all the runs presented in this study, unless otherwise stated. Using these parameters, a steady state topography with a fault throw rate of 0.3 mm/a was generated for the static case (Figures 3, 4). The “modeled steady state Rio Torto” has a channel width $W = 17 \text{ m}$ and a channel slope $S = 0.025$ at the outlet (Figure 4). To produce a channel with similar geometry at steady state when equations (2) and (3) were used, the coefficients k_{wf} and k_{ww} were set to 3.2 and $1.2 \text{ m}^{-1/8} \text{ s}^{3/8}$ respectively. The hydraulic scaling coefficient values presented above were then kept constant in this study. To summarize, three steady state topogra-

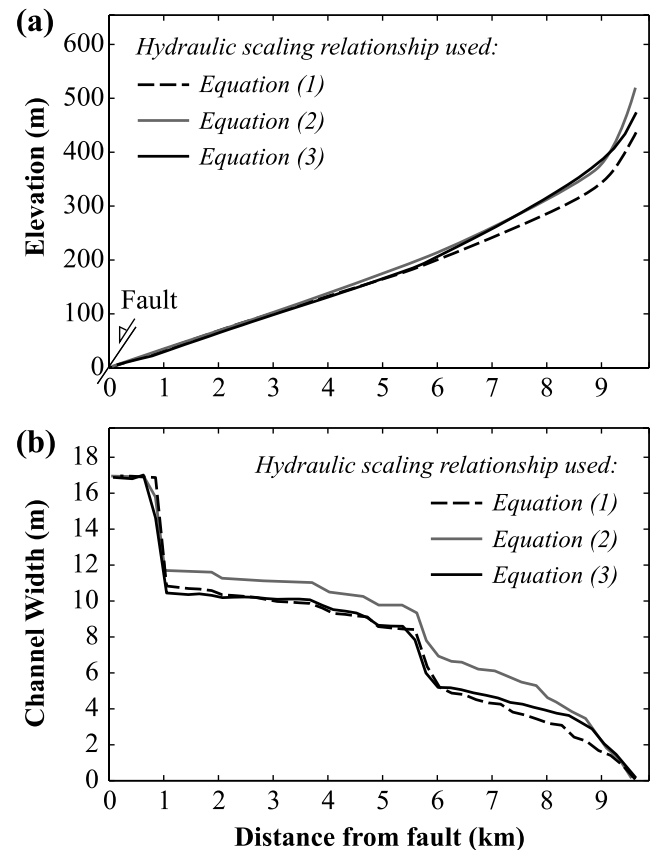


Figure 4. Characteristics of the modeled Eastern channel in steady state with a fault throw rate of 0.3 mm/a, using the typical hydraulic scaling relationship (equation (1), static case), using the Finnegan equation (equation (2), dynamic case), or using the Whittaker equation (equation (3), dynamic case_II). (a) Long profiles and (b) channel width along profile.

phies with a fault throw rate of 0.3 mm/a were produced in the static case, dynamic case and dynamic case_II. The three topographies are characterized by identical width and slope at the outlet, but the steady state profiles slightly

differ upstream, due to minor difference in channel width (Figure 4).

[9] Starting from these similar steady state topographies, the transient response of the landscape to a throw rate increase on the fault from 0.3 to 1.0 mm/a was analyzed (section 5.1). Four series of runs were performed: the channel width was defined either by the typical hydraulic scaling equation (equation (1), static case), by the Finnegan equation (equation (2), dynamic case) or by the Whittaker equation (equation (3), dynamic case_II); the fourth series was performed to examine the first-order effect of varying channel width on landscape development, imposing a constant channel width throughout the channel network. In this case ($W = \text{constant}$), the initial topography generated using equation (1) was used.

[10] Finally, three additional series of runs were performed with varied tectonic forcing and with a shear stress threshold for erosion (sections 5.2, 5.3, and 5.4). The purpose of these runs was to analyze the effect of dynamic channel adjustment in different conditions and draw more generic conclusions which can be applied to any kind of landscape. For these runs, the static case was compared to the dynamic case, the validity of the Whittaker equation (equation (3), dynamic case_II) having been demonstrated only along the Rio Torto.

5. Model Results

5.1. Reference Case

[11] Fault acceleration from 0.3 to 1.0 mm/a causes a 3.3 fold increase in uplift rate over the catchment. The channel responds by increasing its slope (Figures 5a and 5b): from the fault, a steepened reach extends upstream, along which

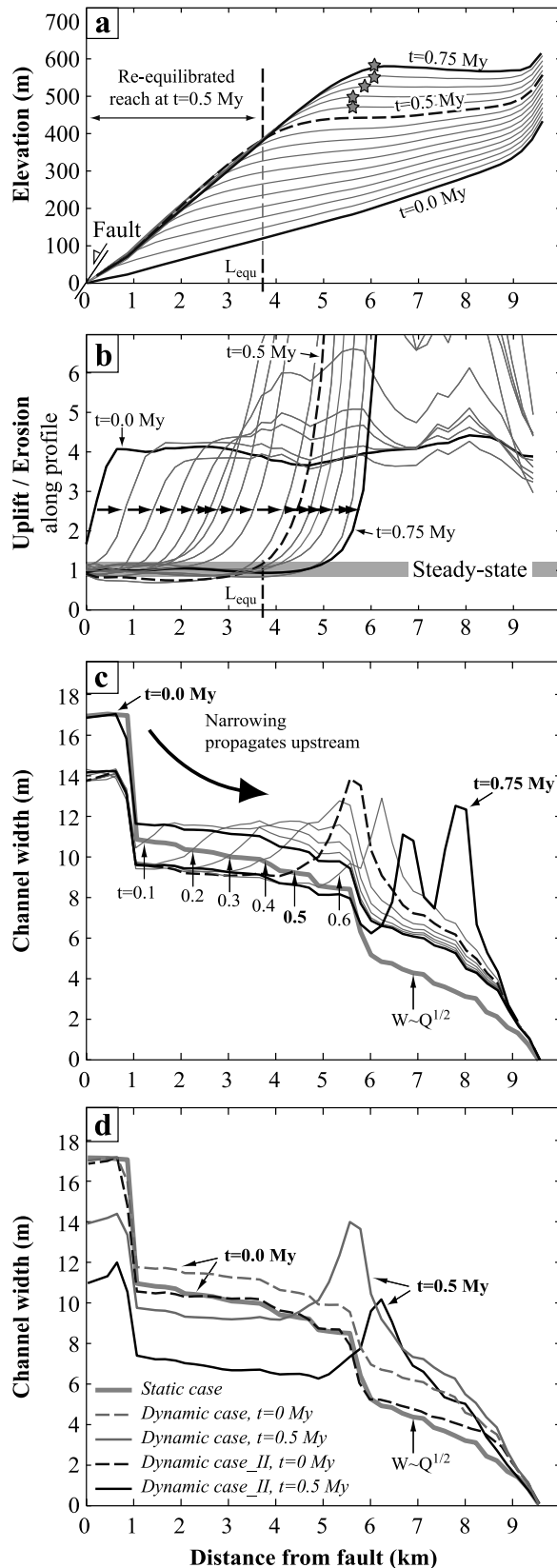


Figure 5. Eastern channel evolution after fault acceleration to 1 mm/a. (a) Profile evolution, using equation (1) (static case). Initial profile in steady state with fault throw rate of 0.3 mm/a is shown at $t = 0.0$ Ma. Time between profiles is 0.05 My. Black thick lines at $t = 0.0$ and 0.75 Ma. Dashed line at $t = 0.5$ Ma; the part of the profile which is re-equilibrated at this time with respect to the new uplift field is indicated (re-equilibrated length L_{equ} , see Figure 5b). Stars indicate negative slope leading to drainage reversal. (b) Evolution of the rock-uplift-to-erosion-rate ratio along the profiles shown in Figure 5a. Time between curves is 0.05 Ma. The length of the re-equilibrated reach (uplift = erosion) increases through time; arrows show the propagation of the “wave of re-equilibration”. Black thick lines at $t = 0.0$ and 0.75 Ma. Dashed line at $t = 0.5$ Ma (re-equilibrated length L_{equ}). (c) Evolution of channel width along profile when equation (2) is used (dynamic case). Time between curves is 0.1 Ma. Numbers indicate time in Ma. Black thick lines at $t = 0.0$ and 0.75 Ma, dashed line at $t = 0.5$ Ma. Thick grey line indicates channel width using equation (1) (static case). (d) Evolution of channel width along profile when equation (2) (dynamic case) or equation (3) (dynamic case_II) is used. Curves at $t = 0$ (dashed lines) and 0.5 Ma (solid lines) are represented in both cases, showing the importance of channel narrowing associated with increase in slope. Thick grey line indicates channel width using equation (1) (static case).

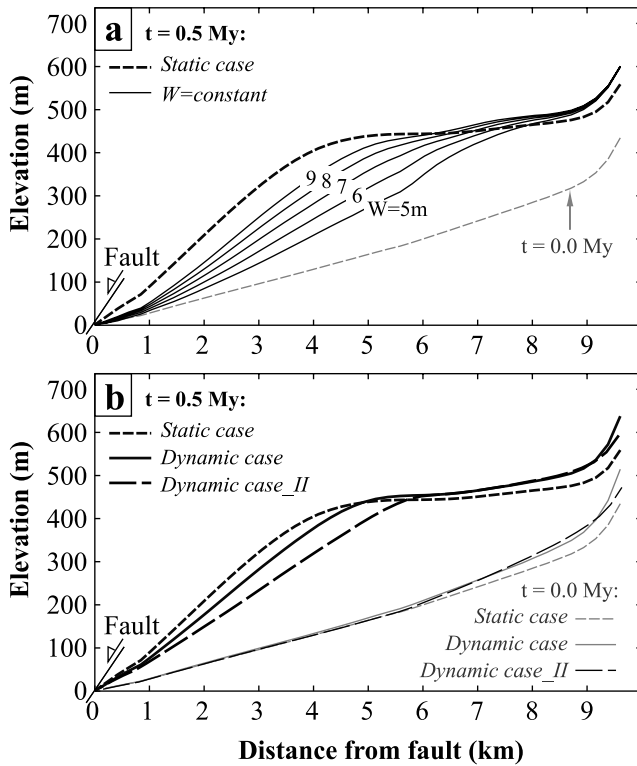


Figure 6. Modeled profiles 0.5 Ma after fault acceleration, using different hydraulic scaling relationships: (a) equation (1) (static case), and $W = \text{constant}$ (W in meter is indicated on the profiles). Initial steady state profile before fault acceleration is also displayed ($t = 0$ Ma). To produce the same erosion rate, a narrow channel requires lower slopes than a wide channel, because it focuses more of its erosive power. (b) equation (1) (static case), equation (2) (dynamic case) and equation (3) (dynamic case_{II}). Initial steady state profiles before fault acceleration are also displayed ($t = 0$ Ma). Channel narrows when slope increases in the dynamic cases: slopes lower than in the static case are consequently produced, particularly in the dynamic case_{II} which predicts a more dramatic narrowing than the dynamic case.

steady state is attained with respect to the new uplift field (called the re-equilibrated reach hereafter). The length of the re-equilibrated reach increases through time, while the upper part of the profile is uplifted and back-tilted, potentially leading to drainage reversal. In the static case, the increase in erosion rate to a value that matches the new uplift rate is axiomatically achieved only by an increase in slope. In the dynamic case and dynamic case_{II}, the increase in slope is also associated with a narrowing of the channel in the lower reach, while the back-tilting of the upper reach results in a slope reduction and a subsequent channel widening (Figures 5c and 5d). Note that the channel narrowing in the dynamic case_{II} is more dramatic than in the dynamic case (Figure 5d). The influence of channel width on the development of the profile is shown in Figure 6: to produce the same erosion rate, a narrow channel requires lower slopes than a wide channel, because it focuses more of its erosive power. Consequently, equation (1) predicts higher channel slope compared to equa-

tions (2) and (3) which allow for dynamic channel adjustment. Over the 2-km-long reach located 1 to 3 km upstream of the fault, the average slope produced in the dynamic case and dynamic case_{II} is respectively 10 % and 30 % lower than the slope produced in the static case, leading to difference in elevation of ~ 20 m and ~ 70 m over a length of 2 km respectively. Note that we chose to present our results (e.g., Figure 5a) as a function of downstream distance, using linear axes, rather than as slope-area log-log plots. The reason for this is that the log-log plots of our results are noisy and thus difficult to interpret, partly because of the limited range of drainage area that we model and also because the rivers do not flow exactly perpendicularly to the fault so the uplift field does not decrease regularly upstream. Whittaker *et al.* [2008] analyze slope-area log-log plots for various catchments in the Apennines (including the Rio Torto catchment) and discuss the problems associated with this type of representation in this context.

[12] Channel width also exerts an important control on the response time of the system. Equation (7) can be written as follows:

$$dz/dt \sim K_5(Q/W)dz/dx, \quad (10)$$

where z = elevation, t = time, x = longitudinal distance and K_5 = constant. This is a wave equation in which the wave speed is given by $C = K_5(Q/W)$: consequently, the narrower a channel, the faster it responds to the disturbance [see also Stark, 2006]. This is illustrated by Figure 7 which shows the evolution of the length of the re-equilibrated reach (see Figures 5a and 5b) through time. The steeper the slope of a curve in Figure 7, the faster the wave of re-equilibration propagates upstream. The re-equilibrated reach produced in

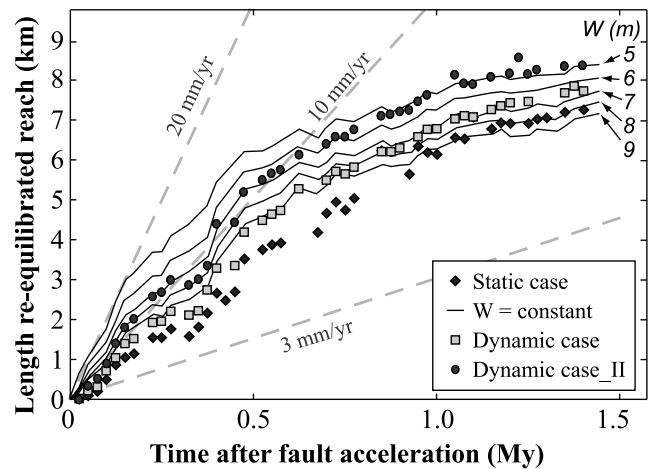


Figure 7. Evolution through time of the length of the re-equilibrated reach upstream of fault, for the Eastern channel, using different expressions for channel width. Channel width is indicated on top right corner for the curves corresponding to the case $W = \text{constant}$. For comparison, dashed lines refer to a wave of re-equilibration propagating upstream at a constant rate. Response time of the system is highly dependent on channel width. The same seed for random storm generation is used for all the runs and is the main source of noise in this diagram.

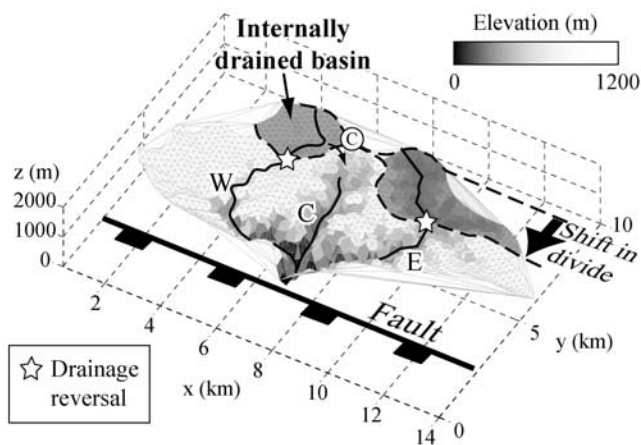


Figure 8. Modeled morphology of a catchment which has experienced drainage reversal (e.g., 0.65 Ma after fault acceleration in the static case). Shaded area represents internally drained basin. Drainage reversal is equivalent to a shift in drainage divide (dashed line) toward the fault. Circled C with arrow illustrates the capture event occurring at $t = 0.875$ Ma in the static case (see text). W, C, and E refer to Western, Central, and Eastern channels respectively.

the static case is systematically shorter than the one produced in the dynamic case (up to 25 % shorter, e.g., at $t = 0.15$ Ma), as the equation (2) allows the channel to narrow as the slope increases. The difference in length reaches ~ 1 km at $t = 0.75$ Ma. When the static case is compared with the dynamic case II, the differences are doubled: the re-equilibrated reach is 50 % shorter at $t = 0.15$ Ma and the difference in length reaches ~ 2 km at $t = 0.75$ Ma.

[13] The differences above influence significantly the resulting landscape morphology. In particular, we focus on the drainage reversal (channel slope < 0) that happens in the upper part of the catchment as a result of back-tilting (Figure 8, see also Figure 5a). Such an event, which has been documented in extensional settings including the Apennines [e.g., Whittaker et al., 2007b], can have a significant impact in terms of landscape development, because the river loses a significant part of its contributing drainage area and has consequently much less stream power to incise. Figure 9 describes the timing and magnitude of the drainage reversal event. Data produced using a constant channel width shows that the narrower the channel, the later the event occurs (Figure 9a). If the channel is narrow enough, no drainage reversal occurs (e.g., Eastern channel with $W = 5$ or 6 m). The drainage area lost is also a function of channel width (Figure 9b): narrow channels tend to lose less drainage area than wide channels, i.e., they involve a less dramatic shift in drainage divide toward the fault (Figure 8). In our model, the drainage divide subsequently migrates away from the fault after drainage reversal occurred, due to regressive erosion. Narrow channels drive a faster rate of divide migration than wide channels and manage consequently to restore their initial drainage area earlier than wide channels (Figure 9b). Note that these model runs assume that lakes form in closed depressions and spill out at the lowest available point on the lake perimeter, which in this case routes water down the main

channels. If instead water entering closed basins was assumed to either evaporate or exit along the watershed perimeter, there would be an immediate reduction in the rate of incision along the beheaded channel and a consequent decrease in the rate of headward migration of the steep reach.

[14] In the static case, the Eastern channel experiences drainage reversal at $t = 0.525$ Ma, that is 25 % earlier than in the dynamic case and 30 % earlier than in the dynamic case II (Figure 9a). The drainage area lost is also more significant in the static case: 37 %, versus 22 % and 10 % of drainage area lost in the dynamic case and dynamic case II respectively (Figure 9b). The time needed for the channel to restore its initial drainage area in the static case is also 70 % longer than in the dynamic case and 150 % longer than in the dynamic case II (Figure 9b). Note that these differences are mostly associated with the propagation of the wave of

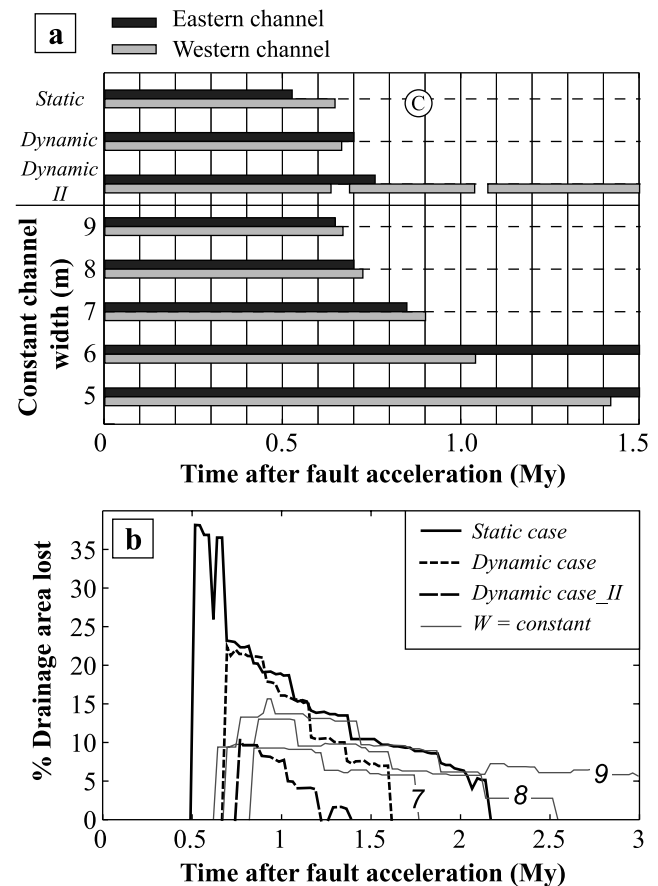


Figure 9. (a) Timing of drainage reversal as a function of the method used to derive channel width: static case (equation (1)), dynamic case (equation (2)), dynamic case II (equation (3)), or $W = \text{constant}$. Box is interrupted when the upper part of a subcatchment becomes internally drained. “C” represents the capture event illustrated in Figure 8. (b) Evolution through time of lost drainage area with respect to initial contributing drainage area for the Eastern channel (Eastern channel is used because of its stability). Channel width is indicated on curves corresponding to the case $W = \text{constant}$. Note the change in scale on the x axis.

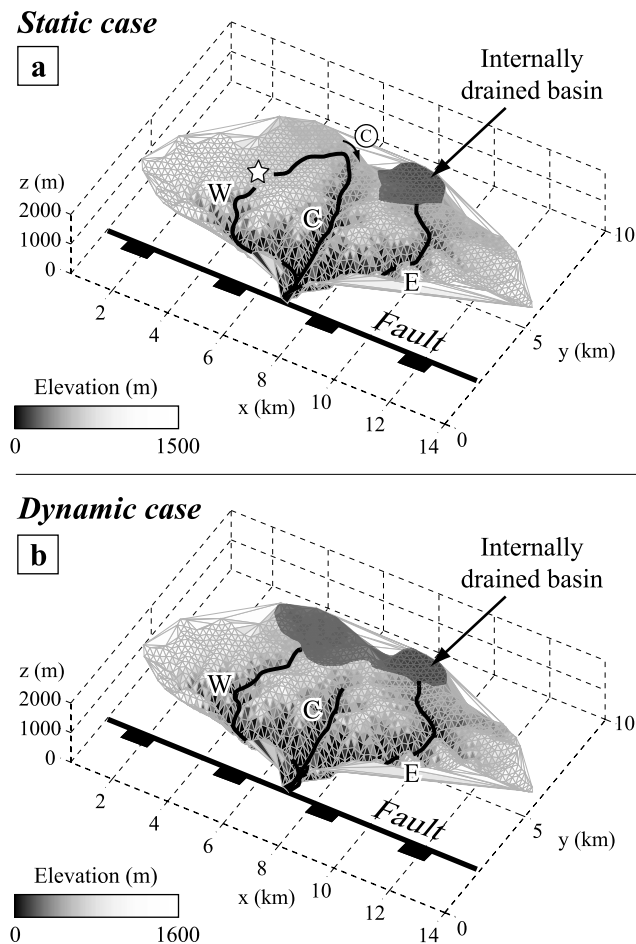


Figure 10. Modeled catchment morphology 1.2 Ma after fault acceleration, in (a) the static case and (b) the dynamic case. Shaded area represents internally drained basin. Circled “C” with arrow illustrates the capture event occurring at $t = 0.875$ Ma in the static case; star represents the resulting windgap. W, C, and E refer to Western, Central, and Eastern channels respectively. Dynamic channel adjustment favors headward erosion along the mainstreams, leading to smaller internally drained basin on the Eastern side of the catchment and preventing the capture event from occurring on the Western side of the catchment.

re-equilibration through the catchment, which is faster when the channel dynamically adjusts. Indeed, dynamic channel adjustment in the back-tilted upper part of the catchment promotes drainage reversal, as channel slope reduction leads in this case to channel widening (Figures 5c and 5d) and consequently to less focused erosion and more dramatic reduction in erosion rate than in the static case. Comparison for the Western channel is more complex. Drainage reversal occurs sporadically in the dynamic case II: the Western channel loses less than 10 % of its contributing area but recaptures it almost “instantly” at $t = 0.65$ and 1.05 Ma (gaps in the Western channel box in Figure 9a). Drainage reversal occurs at approximately the same time in the static and dynamic cases. However, the central channel captures the upper part of the Western channel’s contributing area at $t = 0.875$ Ma in the static case (Figures 8, 9a, 10). The upper part

of the Western catchment has been internally drained for more than 0.2 Ma and water eventually overflows the drainage divide between the central and Western channel, a result of back-tilting and slow erosive regression along the Western channel. In this case, the central channel becomes a more important fluvial feature than the Western channel which is reduced to a second order tributary. A windgap remains where drainage reversal occurred initially (star in Figure 10). It stays perched over time because of a low erosion rate. This leads to very distinct morphologies for the Western part of the catchment, according to the equation used to derive channel width (Figure 10).

5.2. Influence of Uplift Rate After Fault Acceleration

[15] In this section, we analyze the transient response of the landscape to fault acceleration, from 0.3 mm/a to varied throw rates ranging between 0.5 and 1.25 mm/a. The topographies generated in the static case and in the dynamic case are compared. In both cases and as in the reference case, the initial topographies are in steady state with the uplift field associated with a fault throw rate of 0.3 mm/a. The throw rate is then increased to 0.5, 0.75, 1, or 1.25 mm/a (1 mm/a representing the reference case). In response to fault acceleration, a steepened reach extends upstream, as observed in the reference case (Figure 5a). The slope of the steepened reach depends on the new uplift rate (Figure 11a): the higher the uplift rate, the steeper the channel. As a result, the differences between the static and dynamic cases are accentuated with increasing uplift rate: in the static case, the average slope of the steepened reach is just a few percent higher than in the dynamic case for a throw rate of 0.5 mm/a; this difference reaches 15 % when the throw rate is 1.25 mm/a, due to steeper channel and thus more dramatic channel narrowing in the dynamic case.

[16] Despite dramatic differences in channel slope, the velocity of the wave of re-equilibration is independent of the new uplift rate: all runs in the static and dynamic cases produce plots identical to the ones shown in Figure 7 in the static and dynamic cases (section 5.1). The occurrence and magnitude of drainage reversal events is controlled by the competition between headward erosion and the progressive uplifting and back-tilting of the upper part of the catchment. Increasing throw rates on the fault leads to more significant uplifting and back-tilting of the upper part of the catchment. Because, for a given case, the velocity of the wave of re-equilibration is nearly independent of throw rate, high throw rates tend to promote drainage reversal (Figure 11b), leading to early and large drainage reversal events. No drainage reversal occurs when the fault accelerates to 0.5 mm/a. For a throw rate of 0.75 mm/a, the Eastern catchment loses ~13 % of its drainage area in the static case, whereas a faster response of the landscape in the dynamic case prevents the event from occurring. For a throw rate of 1 mm/a (reference case), drainage reversal occurs later and drainage area lost is much smaller in the dynamic case than in the static one (section 5.1). Finally, a throw rate of 1.25 mm/a leads to a dramatic drainage reversal event 0.3 Ma after fault acceleration, during which the catchment loses more than 60% of its drainage area in both cases. In a real setting, such an event is likely to compromise the river’s ability to flow across the fault (see section 6.1), and neither the static case

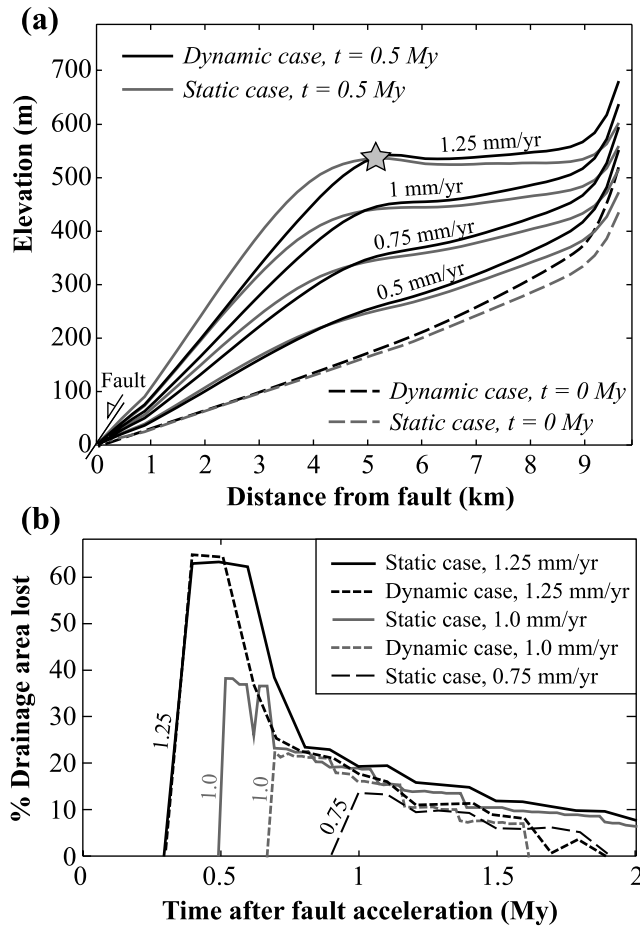


Figure 11. (a) Modeled profiles for the Eastern channel in the static case (grey lines) and dynamic case (black lines), using different values of fault throw rate after acceleration (indicated on the profiles). Initial steady state profiles with fault throw rate of 0.3 mm/a are shown in dashed lines. Profiles 0.5 Ma after fault acceleration are shown in solid lines. Star represents drainage reversal (slope < 0). (b) Evolution through time of lost drainage area with respect to initial contributing drainage area for the Eastern channel, in both static and dynamic cases, for different values of fault throw rate after acceleration (indicated on the curves). The course of the Eastern channel is never reversed in the following cases: dynamic case and throw rate = 0.75 mm/a, static + dynamic cases and throw rate = 0.5 mm/a.

nor the dynamic case allows the catchment to re-equilibrate fast enough to prevent the event from occurring.

5.3. Influence of Pivot Distance

[17] In this section, we analyze the transient response of the landscape to fault acceleration from 0.3 mm/a to 1 mm/a, using different values for pivot distance: the distance between fault and fulcrum is fixed to 10 (reference case), 15, 20, 30 km, and infinity (equivalent to uniform uplift) (Figure 12a). Because the uplift field has changed with respect to the previous runs, new steady state topographies were generated with a throw rate of 0.3 mm/a for each pivot distance, in the static and dynamic cases. The steady state profiles of the “modeled Rio Torto” are shown in the static

case in Figure 12b. For clarity, dynamic case steady state profiles are not represented but, for each pivot distance, the dynamic case profile is slightly above the corresponding static case profile (see Figure 4a for comparison in the reference case with pivot distance = 10 km). Increasing pivot distance is equivalent to increasing the uplift rate in the upper part of the catchment with respect to the lower part of the catchment. As a result, the slopes required to produce erosion rates that match higher uplift rates in the upper part of the catchment are higher. Whereas all steady state profiles are similar near the outlet, they all diverge upstream, the profile with the highest slopes and highest elevations corresponding to the case with the largest pivot distance: uniform uplift (Figure 12b).

[18] In response to fault acceleration, a steepened reach extends upstream of the fault, while the upper part of the catchment is uplifted and back-tilted (Figure 12b). For each case, the profiles 0.5 Ma after fault acceleration are similar

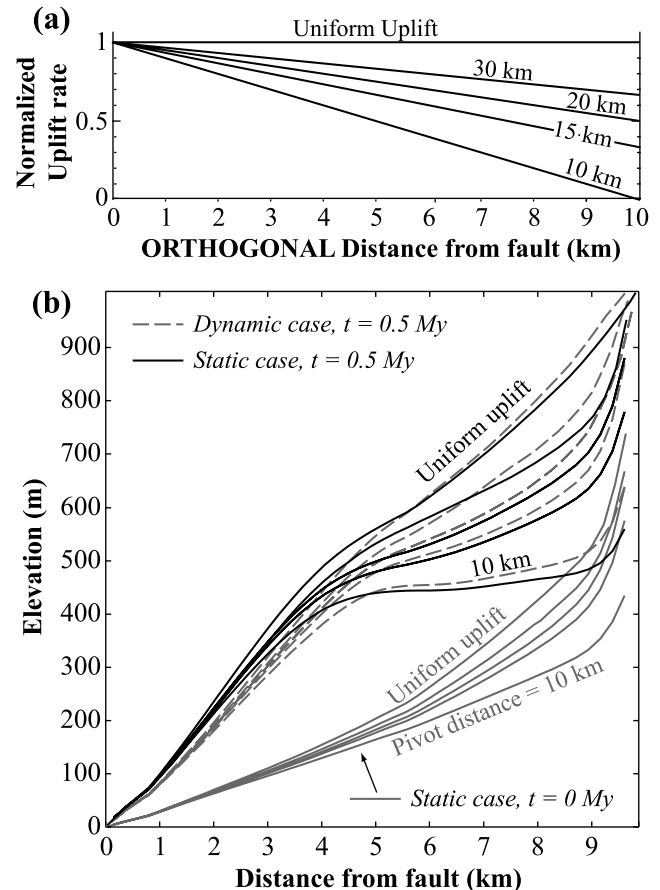


Figure 12. (a) Normalized uplift rate as a function of orthogonal distance from fault for runs using different pivot distances (indicated on curves). (b) Modeled profiles for the Eastern channel for different pivot distances. For clarity, initial steady state profiles are represented only for the static case (solid grey lines). Profiles 0.5 Ma after fault acceleration are represented in the static and dynamic cases (solid black lines and dashed grey lines respectively). The results of 5 runs with different pivot distances are represented: 10 km (lower profile), 15 km, 20 km, 30 km, and uniform uplift (upper profile) respectively.

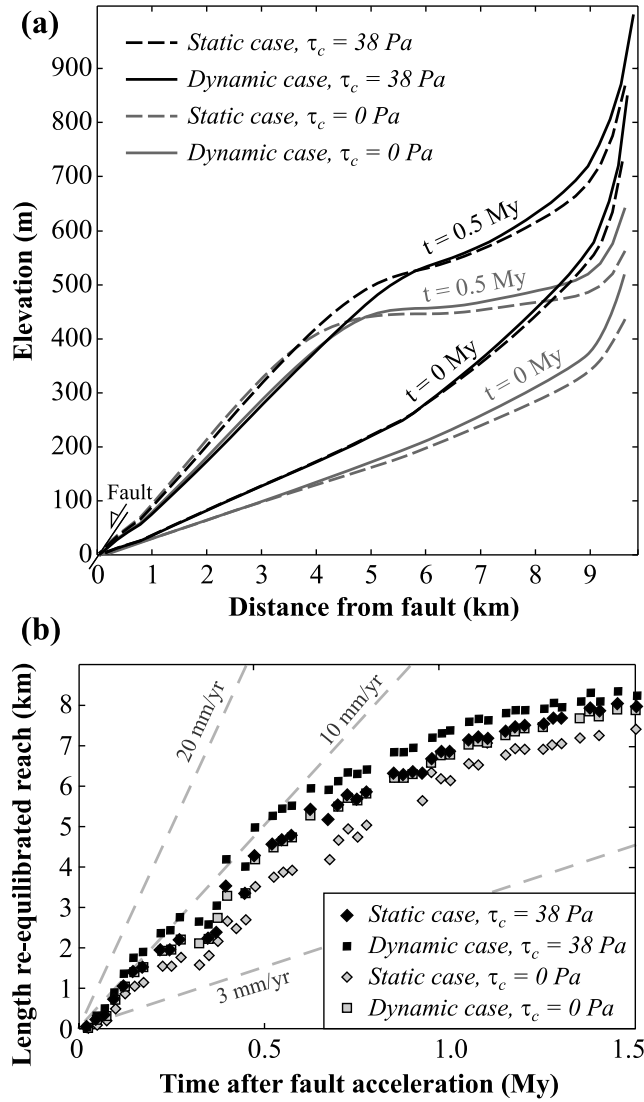


Figure 13. (a) Modeled profiles for the Eastern channel in the *static case* (dashed lines) and *dynamic case* (solid lines), using different values of critical shear stress (τ_c): $\tau_c = 0$ Pa (grey lines) and 38 Pa (black lines). Initial steady state profiles ($t = 0$ Ma) and profiles 0.5 Ma after fault acceleration ($t = 0.5$ Ma) are shown. (b) Evolution through time of the length of the re-equilibrated reach upstream of fault, for the Eastern channel, using different expressions for channel width and different values of critical shear stress (τ_c). For comparison, dashed lines refer to a wave of re-equilibration propagating upstream at a constant rate. The same seed for random storm generation is used for all the runs and is the main source of noise in this diagram.

at the outlet and diverge upstream to compensate for the difference in uplift rate induced by varying the pivot distance. Because slopes are relatively similar along the steepened reach, whatever the pivot distance is, differences in slope between the static case and dynamic case profiles are approximately constant: slope predicted in the static case is systematically $\sim 10\%$ steeper than slope predicted in the dynamic case. In the upper part of the catchment, drainage reversal occurs for a pivot distance of 10 km (reference

case), as described in section 5.1. However, it never happens for values of pivot distance equal to or larger than 15 km. The width of the tilted block exerts consequently a major control on the occurrence of such event: only narrow block are likely to experience drainage reversal, despite a dramatic increase in uplift rate. Finally, pivot distance does not influence the velocity of the wave of re-equilibration: all runs in the static and dynamic cases produce plots almost identical to the ones shown in Figure 7 in the static and dynamic cases (section 5.1).

5.4. Influence of Shear Stress Threshold for Erosion

[19] It is now widely recognized that thresholds for fluvial erosion exist in nature and that they can modulate erosion rates, mostly when associated with stochastic rainfall distribution [e.g., *Snyder et al.*, 2003b; *Tucker*, 2004; *Lague et al.*, 2005]. In this section, we analyze how the introduction of an erosion threshold affects the transient response of our catchment as it responds to fault acceleration. In this case, equation (4) (section 3) becomes:

$$E = k_b(\tau - \tau_c)^p \text{ when } \tau > \tau_c \quad (11a)$$

$$E = 0 \text{ when } \tau < \tau_c, \quad (11b)$$

where τ_c = critical shear stress (Pa). No erosion occurs if the fluvial shear stress τ does not exceed the critical shear stress τ_c .

$$\tau_c = \tau_c^* \Delta \rho g D_{50}, \quad (12)$$

where τ_c^* = dimensionless critical shear stress (Shields stress) commonly assumed to be ~ 0.045 for turbulent rough flows [see *Buffington and Montgomery*, 1997], $\Delta \rho$ = difference in density between the fluid and the sediment ($1650 \text{ kg} \cdot \text{m}^{-3}$ for typical crustal rocks), g = acceleration due to gravity and D_{50} = median grain size of the sediment. Using a median grain size of 5 cm as an upper limit for the representative grain size for the Rio Torto [*Whittaker et al.*, 2007b], we obtain $\tau_c = 38$ Pa. The introduction of this value into the model reduces dramatically the erosive efficiency of the river and leads consequently to significantly steeper slopes if the values of all the other parameters are kept constant. Because we wished to keep similar channel geometries with respect to the runs performed without critical shear stress (previous sections), we did not modify the hydraulic scaling coefficients k_w , k_{wf} , and k_{ww} (equations (1), (2), and (3)). Thus the only way to increase the channel erosivity in order to produce, after fault acceleration to 1 mm/a, an average channel slope that matches the average slope over the segment of the Rio Torto that has responded to the fault acceleration (steepened reach with $S \sim 0.1$, see Figure 2) [*Whittaker et al.*, 2007a], was to increase the erodibility coefficient k_b ; the match was achieved for $k_b = 10 \cdot 10^{-6} \text{ m}^{-1/2} \text{ kg}^{-3/2} \text{ s}^2$.

[20] The introduction of a critical shear stress induces a strong nonlinear behavior between slope and erosion rates (Figure 13a): although runs with and without threshold produce similar slopes over the steepened reach after fault acceleration, the initial topographies in steady state with

respect to the uplift rate associated with a fault throw rate of 0.3 mm/a strongly differ. When a threshold is used, the probability for the shear stress associated with a flood to exceed the threshold and produce erosion decreases with decreasing drainage area. Consequently, although k_b has been raised, steeper slopes are needed to compensate for the loss in stream erosivity induced by the introduction of the threshold, mostly in the upper part of the catchment, where the effect of the threshold is more important (small drainage area). The relief of the initial steady state catchment is consequently more important when critical shear stress is specified (Figure 13a).

[21] The transient response of the landscape to fault acceleration is very similar to the response documented in the previous runs: a steepened reach extends upstream of the fault while the upper part of the catchment is uplifted and back-tilted. The relative differences between the static and dynamic cases along the steepened reach are essentially unaffected by the threshold (Figure 13a): average slope in the dynamic case remains $\sim 10\%$ lower than average slope in the static case. In the upper part of the catchment, the enhanced relief produced when a threshold is used delays or prevents drainage reversal (Figure 13a): the Eastern catchment loses $\sim 9\%$ of its drainage area at $t = 1.1$ Ma and regains it in less than 0.1 Ma in the static case; the Western catchment also loses $\sim 20\%$ of its drainage area at $t = 0.9$ Ma in the static case, whereas drainage reversal does not happen at all in the dynamic case. This difference between static and dynamic cases can be explained by the fact that the response time of the landscape is shorter when dynamic channel adjustment occurs (Figure 13b). The introduction of the threshold leads to a faster response of the landscape in both static and dynamic cases but the differences between the two cases in terms of length of re-equilibrated reach and consequently of response time are very similar, whether a threshold is used or not. This can probably be explained by the fact that, over the steepened reach, high slope and relatively high discharge result in high fluvial shear stress which minimizes the effect of the threshold for erosion. For example, the average discharge along the reach between 1 and 4 km upstream of the fault is roughly constant ~ 4.7 m³/s, as drainage area does not vary significantly. Introducing this value and a slope of 0.1 in equation (5) produces a cross-section averaged boundary shear stress of ~ 140 Pa, which is around four times the threshold value.

6. Discussion

6.1. Effect of Dynamic Channel Adjustment on the Transient Response of the Landscape to Fault Acceleration

[22] In our example, the integration of dynamic channel adjustment mostly affects the slope exponent in the stream power law (equations (7), (8), and (9)). While this change does not dramatically affect the steady state topographies and channel widths (Figure 4), it generates different responses when the landscape experiences a tectonic disturbance. The first effect can be seen in channel gradient: in response to fault acceleration from 0.3 to 1 mm/a, the use of the Finnegan equation (equation (2), dynamic case) which allows dynamic channel adjustment assuming that width-to-depth ratio and

bed roughness are constant within the fluvial network [Finnegan *et al.*, 2005], produces slopes $\sim 10\%$ lower than the slopes predicted using the width-discharge scaling relationship (equation (1), static case). The use of the Whittaker equation (equation (3), dynamic case_II) which additionally accounts for the reduction of width-to-depth ratio with increasing slope documented in the Rio Torto catchment [Whittaker *et al.*, 2007a] produces slopes $\sim 30\%$ lower than in the static case. These differences depend on the amplitude of the increase in relative uplift rate: a high increase in uplift rate promotes the development of steep slopes after fault acceleration which in turn produces dramatic channel narrowing in the dynamic cases; the more dramatic the channel narrowing, the more significant the differences in slope between static and dynamic cases (section 5.2). In terms of response time, systematic differences are observed as well, as narrow channels respond faster than wide ones (equation (10)). At a given time after fault acceleration, the length of the re-equilibrated reach, which represents how far in the catchment the wave of re-equilibration has propagated, is systematically larger when the channel dynamically adjusts (Figure 7): the length is up to 25 % shorter in the static case than in the dynamic case, with the difference in length reaching ~ 1 km at $t = 0.75$ Ma; this length is up to 50 % shorter in the static case than in the dynamic case_II, with the discrepancy reaching ~ 2 km at $t = 0.75$ Ma. Importantly, these differences are not significantly influenced by the rate of uplift after fault acceleration, by the pivot distance or by the use of a critical shear stress for erosion (sections 5.2, 5.3, and 5.4 respectively).

[23] Our results demonstrate that these differences can have a significant impact on the pattern of landscape evolution predicted for a catchment experiencing an uplift field typical of many extensional settings. In our example, large differences in the timing and magnitude of the drainage reversal arise for the Eastern channel (Figures 8 and 9). For the Western channel, drainage reversal occurs at the same time in both static and dynamic case, while the catchment responds fast enough in the dynamic case_II to prevent the event from occurring; in addition, a capture event by the central channel occurs only in the static case, which profoundly affects the morphology of the catchment (Figures 8 and 10). These differences result from the fact that, in a normal fault setting, transverse drainage is subject to a delicate balance between base-level lowering at the fault, which drives headward erosion, and back-tilting, which drives the progressive reduction of the slopes in the upper part of the catchment and may lead to drainage reversal [see also Humphrey and Konrad, 2000; Douglass and Schmeeckle, 2007]. This balance is consequently highly dependent on the tectonic forcing experienced by the catchment. The theory predicts that headward erosion is favored if a channel narrows in response to increased gradient (equation (10)); this is verified by our numerical solutions, as the catchment responds faster in the dynamic cases than in the static case. Our results show however that the velocity of the wave of re-equilibration is not significantly influenced by the tectonic setting. It is thus not a surprise that the propensity for a catchment to experience drainage reversal depends mostly on the rate of relative uplift and degree of back-tilting experienced by its headwaters. All else equal, narrow fault blocks with strong slip-

rate acceleration have the greatest potential for drainage reversal [see also *Whittaker et al.*, 2007b].

[24] In the setting considered in this study, we show that dynamic channel adjustment has a significant impact on the modeled transient response of the landscape. This impact is expected to be even larger when considering the regional response of a landscape to active tectonics, where the competition between catchments is strong and where acts of drainage piracy are likely [*Bishop*, 1995; *Brocard and van der Beek*, 2006; *Cowie et al.*, 2006, *Douglass and Schmeeckle*, 2007]. In the present study, the catchment boundary is kept fixed. In reality, a river which experiences drainage reversal is likely to lose completely the upper part of its catchment, due to capture by incising streams from adjacent catchments. The loss of the headwaters would significantly reduce the stream power and hence erosivity of the lower part of the river. In response to this sudden drop in stream power, the river would need to steepen and/or narrow to keep pace with ongoing uplift and back-tilting. Clearly, drainage reversal events leading to a significant reduction in catchment size (e.g., 60% drainage area loss predicted as fault accelerates to 1.25 mm/a, section 5.2) are likely to fatally compromise the channel's ability to incise across the fault. The result would be a small, steep catchment eroding the proximal footwall. In such a scenario, the timing of drainage reversal is thus crucial in controlling landscape evolution. Importantly, this scenario also influences the deposition patterns in the hanging wall basin, as the location of a depocenter depends on whether or not a river is able to transport the sediments across an active fault, from the footwall to the adjacent basin [e.g., *Cowie et al.*, 2006].

6.2. Model and Reality

[25] Because models are not as complex as nature, it is important to discuss the simplifications inherent to the model we have used, and the extent to which they influence the outcomes of our analysis. In this section we therefore outline some of the key limitations of the model and we discuss the extent to which our conclusions are directly comparable to field studies.

[26] While the first-order similarities between the actual and modeled profiles for the Rio Torto (Figures 2 and 6b) are satisfying, there are some interesting discrepancies. For example, the best match to the present-day long profile happens for model runs at $t = 0.5$ Ma, while we know that the Fiamignano fault accelerated 0.75 Ma. Moreover, one could argue that the static case appears to fit the present-day long profile better than the dynamic cases, and that the predicted present-day channel is too narrow in the dynamic case_II (Figures 2, 5d, and 6b). These observations result from the way our calculations were performed: we did not try to simply fit the field data alone, as this could be done relatively easily by adjusting the less well constrained model parameters. For example, if a k_{ww} value of $1.6 \text{ m}^{-1/8} \text{ s}^{3/8}$ is used instead of 1.2 in the dynamic case_II, a channel width of ~ 9 m and a slope of ~ 0.1 are obtained over the steepened reach after fault acceleration, in agreement with field data (Figure 2). A good fit could be obtained with the Finnegan equation as well, and the differences between the three cases would then be very subtle, in terms of catchment morphology and response

time. However, it is neither informative nor surprising to demonstrate that differing combinations of model parameters can generate similar looking landscapes or replicate time-specific field examples. Instead, the strength of our approach is that we generate in our three cases (static, dynamic, and dynamic_II), for a given tectonic forcing, similar steady state topographies with similar channel geometries (section 4), using the field data to determine a “realistic” set of parameters; we then analyze in these three cases the response of the catchment to fault acceleration (section 5). This means the time-dependent transient channel geometries evolve without having to fix key model coefficients to reproduce the present-day geometry, allowing us to compare the effect of dynamic channel adjustment more effectively. By characterizing and quantifying the differences between the time-dependent responses generated in each case, we also generate wider insights into the effects that channel-geometry dynamics have on landscape evolution in extensional settings. This is important because while we know that dynamic channel adjustment is a reality [e.g., *Finnegan et al.*, 2005; *Wobus et al.*, 2006; *Cantelli et al.*, 2007], in particular in the studied catchment [*Whittaker et al.*, 2007a], the geomorphic implications of this on timescales $>10^5$ years have, until now, not been recognized.

[27] In terms of the ‘detachment-limited’ fluvial erosion law (equation (4) and section 3), no consensus exists on the degree to which this law accurately represents erosional dynamics over geologic time, or on the value to which the exponent p should be set. Two main models exist: the “unit stream power” model in which $p = 3/2$, which implies that the rate of incision is proportional to the rate of energy dissipation along the channel, and the “shear stress” model in which $p = 1$, which implies that the rate of incision scales with fluvial shear stress [e.g., *Whipple and Tucker*, 1999]. In this study, we chose the “unit stream power” model ($p = 3/2$) for its simple, near-linear form. Using the “shear stress” model ($p = 1$) would lead to a 33 % reduction of the exponents in the erosion equations (6) to (9); such change would be equivalent to or more significant than the change induced by the introduction of channel adjustment. However, as this change would systematically affect both the slope and drainage area exponents, the importance of slope with respect to drainage area in terms of controlling erosion rate would not be modified. We consequently suspect that our conclusions regarding the importance of dynamic channel adjustment would not be dramatically different if the p exponent were set to unity. Indeed our conclusions have significant implications for any erosion law that explicitly or implicitly includes channel width.

[28] For the sake of simplicity, we derived boundary shear stress using the “wide channel” assumption. However, calculations of bed and bank shear stress with ray-isovel models suggest that peak bed stress is overestimated by equation (5) in channels with width-to-depth ratio (W/D) equal to or lower than ~ 7 [*Shimizu and Itakura*, 1989; *C.W. Wobus et al.*, Modeling the evolution of channel shape: Balancing computational efficiency with hydraulic fidelity, *Journal of Geophysical Research*, 2008]. In the Rio Torto, W/D ranges between 4 and 12 meaning the shear stress is probably overestimated in the narrowest reaches. For a ratio $W/D = 5$, the peak bed shear stress is ~ 75 % of

the shear stress estimated using the wide channel assumption [Shimizu and Itakura, 1989; Wobus *et al.*, submitted manuscript, 2008]. However, we emphasize that the differences in channel width (and thus W/D) between the static case and dynamic case are not large (Figure 5c) so the effect is approximately the same in both cases: i.e., the differences observed between the two cases would not be dramatically affected by the use of an expression of bed shear stress adapted to narrow channels. The amount of narrowing in the dynamic case_II is somewhat larger (Figure 5d) and so the differences documented between the dynamic case_II and the other cases are maximum estimates.

[29] The use of a constant value of critical shear stress representative of the average median grain size in the Rio Torto catchment did not significantly modify our findings (section 5.4), but there are two limitations to note here. First, using the size of loose bed sediments in the Rio Torto to estimate a basin entrainment threshold τ_c represents a minimum choice: the effective threshold stress for detaching or abrading intact bedrock may well be larger. Second, the analysis neglects the possibility of space-time variations in τ_c . The transient response of the landscape in the Rio Torto catchment is, in reality, characterized by a change in sediment grain size associated with a change in the nature of sediment supply to the channel [Whittaker *et al.*, 2007a, 2007b]. Along the steepened reach, a large proportion of the sediment is supplied to the gorge through rockfall and deep-seated landslides, compared to shallower and more diffusive processes in the upper part of the catchment. As a result, grain size is larger along the steepened reach than in the headwaters. This phenomenon might explain the change in width-to-depth ratio documented along the Rio Torto, which led to the definition of equation (3): an increase in grain size provokes an increase in bed roughness, resulting in a decrease in flow velocity and thus width-to-depth ratio. However, such change in grain size should also lead to an increase in critical shear stress for erosion along the steepened reach. We suspect that such a phenomenon would enhance the effect of dynamic channel adjustment. Indeed, a higher critical shear stress along the steepened reach would have to be counterbalanced by higher slopes. Higher slopes would make channel narrowing more dramatic in the dynamic cases, leading to larger differences in slope, width and thus response time between the static and dynamic cases. Further work is needed to characterize and quantify in detail the changes in sediment caliber associated with the transient response of the landscape and to analyze the effects of these changes on landscape development.

[30] In our study, deposition is not modeled. One can consequently question the representativeness of the drainage reversal events documented, aggradation being a way by which rivers can avoid being dammed or diverted [Humphrey and Konrad, 2000; Douglass and Schmeeckle, 2007]. However, we suspect that, in our context, aggradation is limited by a given number of factors. Prior to fault acceleration, the rivers are eroding at a rate matching the initial uplift rate associated with a fault throw rate of 0.3 mm/a. When fault acceleration occurs, the upper reaches of the transverse channels (i.e., upstream of the steepened reach) are progressively back-tilted because of the geometry of the normal fault (Figure 5a). As a result, the erosion rates

along the upper reaches, which were already low prior to fault acceleration due to uplift rate (and thus erosion rate) decreasing with increasing distance from fault, progressively decrease. This reduction of down-cutting rate is seen by tributaries and hillslopes as a reduction of base-level lowering and leads to a decrease in erosion rates all over the upper part of the catchment. As a result, sediment flux also decreases progressively, at a rate which is a function of the response time of the hillslopes and tributaries to adjust to the reduction in down-cutting rate along the trunk channel. Just before drainage reversal occurs, slope angle approaches zero in the main channel, upstream of the steepened reach. Erosion rate is consequently also negligible and aggradation might occur, due to the low transport capacity of the channel. This aggradation could actually favor drainage reversal, as it would be localized where the slope is very low. Subsequently, aggradation might occur in the now internally drained basin. However, as erosion rates are now very low in the upper part of the catchment, sediment fluxes are low as well and the aggradation is unlikely to counterbalance the effect of continuous back-tilting, particularly if the throw rate on the fault is large and/or the tilted block narrow. Field evidence in the Apennines support this history: in the upper part of the Rio Torto catchment, for example, hillslopes dip gently and tend to exhibit convex up profiles testifying to low erosion rates; in addition, there is little evidence for significant sediment supply and transport along the channel [Whittaker *et al.*, 2007a, 2007b]. We also commonly observed internally drained or reversed basins in the Apennines and we suspect that the upper part of the Rio Torto catchment will experience drainage reversal within a few hundreds of thousands of years [Whittaker *et al.*, 2007b]. In some settings, internally drained basins would be filled with water; the lake would overflow over the zone where $S < 0$ and the water gathered in the upper part of the catchment would contribute to runoff at the outlet of the catchment. However, in scenarios where the bedrock is permeable and where the climate is characterized by short-lived intense rainfall events (such as the Apennines), we suspect that internally drained basins will not contribute to runoff until they are captured by neighboring incising streams. Indeed, similar morphologies have been documented in other limestone-dominated landscapes in comparable tectonic settings with a Mediterranean-style climate, such as the South side of the Gulf of Corinth [e.g., Armijo *et al.*, 1996]. We therefore emphasize that the use of a detachment-limited fluvial erosion law in this study (see above) limits the applicability of our results to sediment-starved rivers such as the Rio Torto, as it has been shown theoretically [e.g., Sklar and Dietrich, 2006; Whipple and Tucker, 2002; Gasparini *et al.*, 2006] and in the field [Cowie *et al.*, 2008] that a large sediment supply can considerably affect the way river systems respond to a disturbance.

7. Conclusion

[31] This study demonstrates the potential importance of dynamic channel-width adjustment, particularly when the relative uplift-rate field is nonuniform. In our example, the transient response of a catchment in the footwall of an active normal fault that undergoes an increase in throw rate is modeled using a detachment-limited fluvial erosion law.

On the basis of this scenario, we show that the response of the landscape to an increase in relative uplift rate depends on the degree to which the channel narrows in response to increased gradient. When equations allowing dynamic channel adjustment are used [Finnegan *et al.*, 2005, equation (2); Whittaker *et al.*, 2007a, equation (3)], the transient landscape is characterized by reduced channel gradients and shorter response time than when the simple width-discharge scaling relationship is used [e.g., Leopold and Maddock, 1953, equation (1)]. The differences between models in terms of gradient depend on the magnitude of fault acceleration, whereas the differences in terms of response time are mostly independent of uplift rate and fault pivot distance. In our reference case, channel gradients over the part of the catchment which has responded to fault acceleration are respectively 10 % and 30 % lower in the dynamic case and dynamic case II than in the static case. At a given time after fault acceleration, the length of the re-equilibrated reach, which represents how far in the catchment the wave of re-equilibration has propagated, is up to 25 % shorter in the static case than in the dynamic case, with a difference in length reaching ~ 1 km at $t = 0.75$ Ma; these differences are doubled when static case is compared with dynamic case II. When integrated in three dimensions over the catchment, these discrepancies cause landscape morphologies to differ, particularly with a strong uplift-rate gradient (e.g., narrow tilted blocks) and/or pronounced fault acceleration. The morphological differences, evidenced here at the scale of one catchment, are expected to be more dramatic when the evolution of a whole area composed of adjacent competing catchments is modeled. We consequently recommend the use and introduction into numerical landscape evolution models of a hydraulic scaling law that allows dynamic channel adjustment, particularly when the uplift field is nonuniform. The equation proposed by Finnegan *et al.* [2005] (equation (2)) is supported by theoretical work on development of self-formed channels [Wobus *et al.*, 2006] and represents an improvement in terms of channel width and specific stream power prediction [Whittaker *et al.*, 2007a]. However, it does not appear to fully capture the mechanisms by which bedrock channels adjust their properties in response to change in external forcing such as change in width-to-depth ratio; such changes can noticeably accentuate the differences between “static” and “dynamic” predictions, as shown by the use of the empirical equation proposed by Whittaker *et al.* [2007a] (equation (3)). Further work is consequently needed to fully understand, characterize, and quantify the mechanisms of bedrock channel adjustment.

[32] **Acknowledgments.** This project was funded by the NERC Research grants NE/B504165/1 (Cowie, Roberts, Attal, and Tucker), NER/S/A/2002/10359 (Whittaker), GR9/02995 (Roberts, Michetti), and by ARO and NSF (47033-EV and EAR-0643240; Tucker). We thank Eutizio Vittorio (APAT) for the DEM from which we derived the triangulated irregular network used in the numerical model. We are extremely grateful to Doug Burbank, Noah Finnegan, Dimitri Lague and Alex Densmore for their significant improvement to the manuscript.

References

- Amos, C. B., and D. W. Burbank (2007), Channel width response to differential uplift, *J. Geophys. Res.*, *112*, F02010, doi:10.1029/2006JF000672.
- Anders, M. H., M. Spiegelman, D. W. Rodgers, and J. T. Hagstrum (1993), The growth of fault-bounded tilt blocks, *Tectonics*, *12*, 1451–1459.
- Armijo, R., B. Meyer, G. C. P. King, A. Rigo, and D. Papanastassiou (1996), Quaternary evolution of the Corinth rift and its implications for the late Cenozoic evolution of the Aegean, *Geophys. J. Int.*, *126*(1), 11–53.
- Bishop, P. (1995), Drainage rearrangement by river capture, beheading and diversion, *Prog. Phys. Geogr.*, *19*, 449–473.
- Brocard, G. Y., and P. A. van der Beek (2006), Influence of incision rate, rock strength, and bedload supply on bedrock river gradients and valley-flat widths: Field based evidence and calibrations from western Alpine rivers (southeast France), *Geol. Soc. Am. Spec. Pap.*, *398*, 101–126.
- Buffington, J. M., and D. R. Montgomery (1997), A systematic analysis of eight decades of incipient motion studies, with special reference to gravel-bedded rivers, *Water Resour. Res.*, *33*, 1993–2029.
- Burbank, D. W., J. Leland, E. Fielding, R. S. Anderson, N. Brozovic, M. R. Reid, and C. Duncan (1996), Bedrock incision, rock uplift and threshold hillslopes in the northwestern Himalayas, *Nature*, *379*, 505–510.
- Cantelli, A., M. Wong, G. Parker, and C. Paola (2007), Numerical model linking bed and bank evolution of incisional channel created by dam removal, *Water Resour. Res.*, *43*, W07436, doi:10.1029/2006WR005621.
- Carter, C. L., and R. S. Anderson (2006), Fluvial erosion of physically modeled abrasion-dominated slot canyons, *Geomorphology*, *81*, 89–113.
- Cowie, P. A., M. Attal, G. E. Tucker, A. C. Whittaker, M. Naylor, A. Ganas, and G. P. Roberts (2006), Investigating the surface process response to fault interaction and linkage using a numerical modelling approach, *Basin Res.*, *18*, 231–266.
- Cowie, P. A., M. Attal, A. C. Whittaker, G. P. Roberts, and A. Ganas (2008), New constraints on sediment-flux-dependent river incision: Implications for extracting tectonic signals from river profiles, *Geology*, *36*(7), 535–538, doi:10.1130/G24681A.1.
- Craddock, W. H., D. W. Burbank, B. Bookhagen, and E. J. Gabet (2007), Bedrock channel geometry along an orographic rainfall gradient in the upper Marsyandi River valley in central Nepal, *J. Geophys. Res.*, *112*, F03007, doi:10.1029/2006JF000589.
- Douglass, J., and M. Schmoeckle (2007), Analogue modeling of transverse drainage mechanisms, *Geomorphology*, *84*(1–2), 22–43.
- Duvall, A., E. Kirby, and D. Burbank (2004), Tectonic and lithologic controls on bedrock channel profiles and processes in coastal California, *J. Geophys. Res.*, *109*, F03002, doi:10.1029/2003JF000086.
- Eagleson, P. S. (1978), Climate, soil, and vegetation: 2. Distribution of annual precipitation derived from observed storm sequences, *Water Resour. Res.*, *14*, 713–721.
- Finnegan, N. J., G. Roe, D. R. Montgomery, and B. Hallet (2005), Controls on the channel width of rivers: Implications for modeling fluvial incision of bedrock, *Geology*, *33*, 229–232.
- Finnegan, N. J., L. S. Sklar, and T. K. Fuller (2007), Interplay of sediment supply, river incision, and channel morphology revealed by the transient evolution of an experimental bedrock channel, *J. Geophys. Res.*, *112*, F03S11, doi:10.1029/2006JF000569.
- Gasparini, N. M., R. L. Bras, and K. X. Whipple (2006), Numerical modeling of non-steady-state river profile evolution using a sediment-flux-dependent incision model, *Geol. Soc. Am. Spec. Pap.*, *398*, 127–141.
- Harbor, D. J. (1998), Dynamic equilibrium between an active uplift and the Sevier River, Utah, *J. Geol.*, *106*, 181–194.
- Hawk, K. L. (1992), Climatology of station storm rainfall in the Continental United States: Parameters of the Bartlett-Lewis and Poisson rectangular pulses models, MS Thesis, 330 p., Dep. of Civ. and Environ. Eng., Massachusetts Inst. Tech., Cambridge.
- Howard, A. D. (1994), A detachment-limited model of drainage-basin evolution, *Water Resour. Res.*, *30*, 2261–2285.
- Howard, A. D., W. E. Dietrich, and M. A. Seidl (1994), Modeling fluvial erosion on regional to continental scales, *J. Geophys. Res.*, *99*, 13,971–13,986.
- Humphrey, N. F., and S. K. Konrad (2000), River incision or diversion in response to bedrock uplift, *Geology*, *28*(1), 43–46.
- Johnson, J. P., and K. X. Whipple (2007), Feedbacks between erosion and sediment transport in experimental bedrock channels, *Earth Surf. Processes Landforms*, *32*, 1048–1062.
- Lague, D., N. Hovius, and P. Davy (2005), Discharge, discharge variability, and the bedrock channel profile, *J. Geophys. Res.*, *110*, F04006, doi:10.1029/2004JF000259.
- Lavé, J., and J. P. Avouac (2001), Fluvial incision and tectonic uplift across the Himalayas of central Nepal, *J. Geophys. Res.*, *106*, 26,561–26,592.
- Leopold, L. B., and T. Maddock (1953), The hydraulic geometry of stream channels and some physiographic implications, *U.S. Geol. Surv. Prof. Pap.*, *252*, 56.
- Montgomery, D. R., and K. B. Gran (2001), Downstream variations in the width of bedrock channels, *Water Resour. Res.*, *37*, 1841–1846.
- Roberts, G. P., and A. M. Michetti (2004), Spatial and temporal variations in growth rates along active normal fault systems: An example from The Lazio-Abruzzo Apennines, central Italy, *J. Struct. Geol.*, *26*, 339–376.

- Seidl, M. A., and W. E. Dietrich (1992), The problem of channel erosion into bedrock, *Catena Suppl.*, 23, 101–124.
- Sheperd, R. G., and S. A. Schumm (1974), Experimental study of river incision, *Proc. Vol. Geol. Soc. Am., Parts 1 and 2*, 85, 257–268.
- Shimizu, Y., and T. Itakura (1989), Calculation of bed variation in alluvial channels, *J. Hydrol. Eng.*, 115(3), 367–384.
- Sklar, L. S., and W. E. Dietrich (2006), The role of sediment in controlling steady-state bedrock channel slope: Implications of the saltation–abrasion incision model, *Geomorphology*, 82(1–2), 58–83.
- Snyder, N. P., K. X. Whipple, G. E. Tucker, and D. J. Merritts (2003a), Channel response to tectonic forcing: Field analysis of stream morphology and hydrology in the Mendocino triple junction region, northern California, *Geomorphology*, 53, 97–127.
- Snyder, N. P., K. X. Whipple, G. E. Tucker, and D. J. Merritts (2003b), Importance of a stochastic distribution of floods and erosion thresholds in the bedrock river incision problem, *J. Geophys. Res.*, 108(B2), 2117, doi:10.1029/2001JB001655.
- Stark, C. P. (2006), A self-regulating model of bedrock river channel geometry, *Geophys. Res. Lett.*, 33, L04402, doi:10.1029/2005GL023193.
- Tucker, G. E. (2004), Drainage basin sensitivity to tectonic and climatic forcing: Implications of a stochastic model for the role of entrainment and erosion thresholds, *Earth Surf. Processes Landforms*, 29, 185–205.
- Tucker, G. E., and R. L. Bras (2000), A stochastic approach to modeling the role of rainfall variability in drainage basin evolution, *Water Resour. Res.*, 36, 1953–1964.
- Tucker, G. E., S. T. Lancaster, N. M. Gasparini, R. L. Bras, and S. M. Rybarczyk (2001), An object-oriented framework for distributed hydrologic and geomorphic modeling using triangulated irregular networks, *Comput. Geosci.*, 27, 959–973.
- Turowski, J. M., D. Lague, A. Crave, and N. Hovius (2006), Experimental channel response to tectonic uplift, *J. Geophys. Res.*, 111, F03008, doi:10.1029/2005JF000306.
- Whipple, K. X., and G. E. Tucker (1999), Dynamics of the stream-power river incision model: Implications for height limits of mountain ranges, landscape response timescales, and research needs, *J. Geophys. Res.*, 104, 17,661–17,674.
- Whipple, K. X., and G. E. Tucker (2002), Implications of sediment-flux-dependent river incision models for landscape evolution, *J. Geophys. Res.*, 107(B2), 2039, doi:10.1029/2000JB000044.
- Whipple, K. X., N. P. Snyder, and K. Dollenmayer (2000a), Rates and processes of bedrock incision by the upper Ukak River since the 1912 Novarupta ash flow in the Valley of Ten Thousand Smokes, Alaska, *Geology*, 28(9), 835–838.
- Whipple, K. X., G. S. Hancock, and R. S. Anderson (2000b), River incision into bedrock: Mechanics and the relative efficacy of plucking, abrasion, and cavitation, *Geol. Soc. Am.*, 112, 490–503.
- Whittaker, A. C., P. A. Cowie, M. Attal, G. E. Tucker, and G. P. Roberts (2007a), Bedrock channel adjustment to tectonic forcing: Implications for predicting river incision rates, *Geology*, 35, 103–106.
- Whittaker, A. C., P. A. Cowie, M. Attal, G. E. Tucker, and G. P. Roberts (2007b), Contrasting transient and steady-state rivers crossing active normal faults: New field observations from the Central Apennines, Italy, *Basin Res.*, 19, 529–556, doi: 10.1111/j.1365-2117.2007.00337.x.
- Whittaker, A. C., M. Attal, P. A. Cowie, G. E. Tucker, and G. P. Roberts (2008), Decoding temporal and spatial patterns of fault uplift using transient river long profiles, *Geomorphology*, doi:10.1016/j.geomorph.2008.01.018 (in press).
- Wobus, C. W., G. E. Tucker, and R. S. Anderson (2006), Self-formed bedrock channels, *Geophys. Res. Lett.*, 33, L18408, doi:10.1029/2006GL027182.
- Wohl, E. E., and H. Achyuthan (2002), Substrate influences on incised channel morphology, *J. Geol.*, 110, 115–120.
- Wohl, E. E., and H. Ikeda (1997), Experimental simulation of channel incision into a cohesive substrate at varying gradients, *Geology*, 25, 295–298.

M. Attal, P. A. Cowie, and A. C. Whittaker, Institute of Earth Sciences, School of GeoSciences, University of Edinburgh, West Mains Road, Edinburgh, EH9 3JW, UK. (mikaël.attal@ed.ac.uk)

G. P. Roberts, Research School of Geological and Geophysical Sciences, Birkbeck College, and University College London, Gower Street, London, WC1E 6BT, UK.

G. E. Tucker, Cooperative Institute for Research in Environmental Sciences, and Department of Geological Sciences, University of Colorado, 2200 Colorado Avenue, Campus Box 399, Boulder, CO 80309-399, USA.